TWENTYFIFTH EUROPEAN ROTORCRAFT FORUM

Paper n° H12

OPTIMIZATION-BASED INVERSE SIMULATION OF A HELICOPTER SLALOM MANEUVER

BY

ROBERTO CELI
UNIVERSITY OF MARYLAND, COLLEGE PARK, USA

SEPTEMBER 14-16, 1999
ROME
ITALY

ASSOCIAZIONE INDUSTRIE PER L'AEROSPAZIO, I SISTEMI E LA DIFESA
ASSOCIAZIONE ITALIANA DI AERONAUTICA E ASTRONAUTICA

OPTIMIZATION-BASED INVERSE SIMULATION OF A HELICOPTER SLALOM MANEUVER

Roberto Celi[1]
Department of Aerospace Engineering
Glenn L. Martin Institute of Technology
University of Maryland, College Park, USA

Abstract

This paper presents an inverse simulation methodology based on numerical optimization. The methodology is applied to a simplified version of the slalom maneuver in the ADS-33D helicopter handling qualities specification. The inverse simulation is formulated as an optimization problem with trajectory and dynamic constraints, pilot inputs as design variables, and an objective function that depends on the specific problem being solved. A maximum speed solution is described in the paper. The results show that numerical optimization is a reliable and flexible tool for inverse simulation, both when the required trajectory is prescribed explicitly and when it is defined indirectly through geometric and dynamic constraints. When the trajectory is defined indirectly, there is not a single acceptable trajectory, but rather an entire family with noticeable differences in the helicopter dynamics and in the required pilot inputs. Even when the trajectory is prescribed explicitly multiple solutions exist. For handling qualities studies, the multiple solutions may provide an indication of the amount of scatter in pilot ratings to be expected for a given aircraft and a given maneuver. However, if the inverse simulation is used for simulation validation, then additional constraints may have to be placed on the solution to make it unique.

Notation

V	Flight speed along the trajectory
x	Distance along the centerline of the maneuver, Figure 1
y	Lateral displacement from the centerline of the maneuver (positive to the right), Figure 1
$y_k(x)$	Trajectory that clears the 500 and 1000 ft markers with $y = k$ ft lateral displacement
y_{500}	Lateral displacement for $x = 500$ ft
z	Altitude change from reference value (positive down)
θ_{1c}, θ_{1s}	Lateral and longitudinal cyclic pitch, relative to trim values
θ_0, θ_{0t}	Collective pitch of main and tail rotors, relative to trim values
ϕ	Roll attitude of the helicopter

[1]Associate Professor, Alfred Gessow Rotorcraft Center; e-mail: celi@eng.umd.edu.

1. Introduction

Favorable handling qualities are a key objective of the design of military and commercial helicopters alike. In fact, reducing piloting effort improves mission effectiveness and enhances safety. Extensive effort has gone into the formulation of criteria that relate subjective pilot opinions to quantitative measures of the behavior of a helicopter. The ADS-33D handling qualities requirements [1] are a notable example. Besides a variety of time- and frequency-domain criteria, ADS-33D includes a series of demonstration maneuvers "to provide an overall assessment of the rotorcraft's ability to perform certain critical tasks" [1]. The computer simulation of these maneuvers has received considerable attention in the last few years. The problem is generally formulated as an *inverse* simulation, that is, the required trajectory of the helicopter is prescribed, and the solution consists of the time-histories of the pilot inputs that make the helicopter fly that trajectory. Therefore, inverse simulation could become a useful tool to assess the maneuverability and agility characteristics of a helicopter, piloting workload, and performance limits.

One approach to the solution of the inverse simulation problem consists of recasting it into an optimal control problem [2] by minimizing, using gradient methods, a performance index containing the difference between required and achieved flight path, and augmented with the aircraft ordinary differential equations (ODE) of motion. Another method, developed by Thomson and Bradley [3, 4], resembles a trim calculation carried out at each time step. The sequence in which states and controls are updated, and the update equations, are based on physical and kinematic considerations. Ref. [3] is based on a 6-degree of freedom model. The same basic technique has been used by Whalley [5] in an interesting study that included a validation through a series of piloted simulation experiments. Hess *et al.* [6, 7] have proposed an alternate technique, in which the trajectory is divided into small steps; for a given step the initial controls are known, and the equations of motion are integrated with guesses of the controls at the end of the step. The errors between actual and desired trajectories are calculated, and the controls at the end of the step are adjusted using a Newton-Raphson technique to reduce the errors to zero. This technique is named "integration inverse method", as opposed to the "differentiation inverse method" of Ref. [3] (which requires the differentiation of the desired trajectory). The same technique has been used by Rutherford and Thomson [8] and compared with that of Ref. [3]. The integration method was

found to be an order of magnitude slower than the differentiation method, but more flexible and convenient to set up. The two methods showed comparable accuracy.

Ref. [8] discusses the occurrence of numerical instabilities in both the differentiation and the integration inverse simulation algorithms. De Matteis *et al.* [9] propose a variation of the algorithm of Ref. [6], in which the Newton-Raphson solution at every time step is replaced by a local optimization problem. This technique eliminates some numerical instabilities observed in Ref. [6]. Lee and Kim [10] formulate the inverse simulation as an optimization problem with equality constraints. A variational approach is used to derive optimality conditions, and a method of finite elements in time is used to discretize the resulting equations. Borri *et al.* [11] transform the equations of motion of the aircraft into algebraic equations using finite elements in time. The trajectory constraints are also expressed in algebraic equation form. The combined system is solved using a Newton-Raphson technique. Finally, Yip and Leng have provided stability tests for the integration method applied to time-invariant systems [12]. Refs. [9]-[12] do not address helicopter problems. Except for Ref. [8], the studies previously mentioned do not take rotor dynamics into account.

When inverse simulation is used for helicopter handling qualities studies, it is not immediately obvious which specific trajectory should be prescribed. In fact, for example, ADS-33D does not indicate precise trajectories for the demonstration maneuvers. Instead, it requires that certain geometric and dynamic conditions be satisfied. For example, the slalom of Paragraph 4.2.6 requires that the turns extend from between 50 and 100 ft from the centerline [1], and that the speed be of at least 60 knots. One of the conclusions of Ref. [5] is that there is no guarantee that a preassigned aircraft trajectory is optimal, and a pilot could perform the maneuver better than the inverse simulation would suggest. This conclusion applies to all the studies previously described because in all cases the trajectory is fixed.

In light of the preceding discussion, the main objectives of the paper are:

1. To present a new methodology for inverse simulation, based on the use of numerical optimization. This methodology differs from those mentioned earlier because it operates on a *family* of possible trajectories (and therefore of pilot command time histories) among which it selects the best, based on one or more performance criteria. Traditional inverse simulation with fixed prescribed trajectory can be recovered as a special case.

2. To describe the application of this methodology to a simplified version of one of the ADS-33D demonstration maneuvers, namely the slalom maneuver of Paragraph 4.2.6 of the specification.

3. To discuss some theoretical aspects and practical implementation issues of the proposed methodology.

2. Simulation model

The mathematical model of the helicopter used in this study is a nonlinear blade element type model that includes fuselage, rotor, and main rotor inflow dynamics. The 6 degree of freedom rigid body motion of the aircraft is modeled using nonlinear Euler equations. Linear aerodynamics is assumed for fuselage and empennage. The blades are assumed to be rigid, with offset hinges and root springs. Flap and lag dynamics of each blade are modeled. The main rotor has four blades. The configuration parameters are representative of a hingeless rotor helicopter similar to the BO-105.

The coupled system of rotor, fuselage, and inflow equations of motion is written in first-order form. The state vector has a total of 31 elements: flap and lag displacements and rates for each of the 4 blades (16 states); 12 rigid body positions, velocities, rates, and attitudes; and 3 inflow states. The trim procedure is the same as in Refs. [13, 14]. Thus, the rotor equations of motion are transformed into a system of nonlinear algebraic equations using a Galerkin method. The algebraic equations enforcing force and moment equilibrium are added to the rotor equations, and the combined system is solved simultaneously. The solution yields the harmonics of a Fourier series expansion of the rotor degrees of freedom, the pitch control settings, trim attitudes and rates of the entire helicopter, and main and tail rotor inflow. The free flight maneuver simulation is carried out by integrating the nonlinear equations of motion with the variable-step, variable-order solver DASSL [15, 16].

3. General formulation of the inverse simulation problem

The inverse simulation problem is formulated in nonlinear mathematical programming form. Therefore, the objective is to determine a vector $\mathbf{X}$ of design variables that minimizes a scalar objective function $F(\mathbf{X})$, subject to constraints $g_j(\mathbf{X}) \leq 0, j = 1, \ldots, M$.

The vector of design variables is composed of the values of 4 pilot inputs, namely collective pitch, longitudinal cyclic pitch, and lateral cyclic pitch for the main rotor and collective pitch for the tail rotor, at preassigned time points during the maneuver, that is:

$$\begin{aligned}\mathbf{X}^T = \; & [\theta_0(t_1)\ \theta_{1c}(t_1)\ \theta_{1c}(t_1)\ \theta_{0t}(t_1)\ldots \\ & \ldots\theta_0(t_n)\ \theta_{1c}(t_n)\ \theta_{1c}(t_n)\ \theta_{0t}(t_n)] \qquad (1)\end{aligned}$$

In this study, the times $t_k, k = 1, \ldots, n$ will be equispaced, but need not be. The controls are assumed to vary linearly between consecutive time points; at the initial time T_0 they are set to their respective trim value. Therefore, the number of design variables is equal to $N = 4n$.

The constraints are defined based on the description of the slalom maneuver in Paragraph 4.2.6 of the ADS-33D handling qualities specification [1]. The suggested maneuver is shown in Figure 1. The present study will address a simplified version of the maneuver, with only one excursion to the right of the centerline and one to the left, instead of two, and a total length of 1500 ft along the centerline instead of 2500 ft. Two types of constraints appear in the problem. The first consists of constraints that are enforced at only one point in space or time. The second consists of constraints that are functions of space or time, and that have to be satisfied over the entire maneuver. The constraints enforce the following requirements:

1. The turns must be at least 50 feet from the centerline at 500 and 1000 feet. This results in the two point constraints:

$$g_1(\mathbf{X}) = 1 + \frac{y(t)}{50} \leq 0 \qquad \text{for } t \text{ when } x = 500 \text{ ft} \tag{2}$$

$$g_2(\mathbf{X}) = 1 - \frac{y(t)}{50} \leq 0 \qquad \text{for } t \text{ when } x = 1000 \text{ ft} \tag{3}$$

The quantities x and y are respectively the position along the axis of the maneuver (e.g., along a runway), and the axis perpendicular to it (see Figure 1).

2. The turns must be no more than 100 feet from the centerline at 500 and 1000 feet. This results in the two additional point constraints:

$$g_3(\mathbf{X}) = -1 - \frac{y(t)}{100} \leq 0 \qquad \text{for } t \text{ when } x = 500 \text{ ft} \tag{4}$$

$$g_4(\mathbf{X}) = -1 + \frac{y(t)}{100} \leq 0 \qquad \text{for } t \text{ when } x = 1000 \text{ ft} \tag{5}$$

3. The desired performance calls for an airspeed of at least 60 knots during the entire maneuver, which is expressed mathematically in the form:

$$g_A(\mathbf{X};t) = 1 - \frac{V(t)}{60} \leq 0 \tag{6}$$

where $V(t)$ is the velocity of the helicopter in knots. While the previous constraints were enforced at only specified points of the trajectory, this is a continuous constraint that must be satisfied throughout the maneuver. In this study the constraint is collapsed into one number, which is the integral of the violation over the entire maneuver

$$g_5(\mathbf{X}) = \int_0^T < g_A(\mathbf{X};t) >^2 \, dt \leq 0 \tag{7}$$

where the bracket function is defined as

$$< g_A(\mathbf{X};t) >= \begin{cases} g_A(\mathbf{X};t) & \text{for } g_A(\mathbf{X};t) \geq 0 \\ 0 & \text{for } g_A(\mathbf{X};t) < 0 \end{cases} \tag{8}$$

and the integrand is squared to make the gradient of $g_5(\mathbf{X})$ continuous.

4. A criterion from the previous version of the specification, ADS-33C, called for changes not greater than 10 ft from the reference altitude during the maneuver. Although the current ADS-33D specification no longer includes this criterion, the ADS-33C limits were implemented anyway. If the maneuver starts at a reference altitude z_{ref} this implies that $z_{ref} - \Delta z \leq z(t) \leq z_{ref} + \Delta z$, with $\Delta z = 10$ ft. For convenience, the reference altitude in this study is set to zero, which results in the constraints:

$$g_B(\mathbf{X},t) = -\frac{z(t)}{\Delta z} - 1 \leq 0 \qquad g_C(\mathbf{X}) = \frac{z(t)}{\Delta z} - 1 \leq 0 \tag{9}$$

These two constraints are defined over the entire maneuver and are collapsed into point constraints in the same way as for $g_5(\mathbf{X})$, Eq. (7), which gives

$$\begin{aligned} g_6(\mathbf{X}) &= \int_0^T < g_B(\mathbf{X};t) >^2 \, dt \leq 0 \\ g_7(\mathbf{X}) &= \int_0^T < g_C(\mathbf{X};t) >^2 \, dt \leq 0 \end{aligned} \tag{10}$$

5. The heading angle ψ is required to be within an upper and a lower bound throughout the maneuver. This requirement is not in ADS-33D, and is included to avoid solutions that are mathematically acceptable but practically meaningless, such as a helicopter performing the maneuver while continuously spinning about its yaw axis. Therefore, the absolute value of the heading is required to be less than 45 degrees, which results in the following two continuous constraints:

$$g_D(\mathbf{X},t) = -\frac{\psi(t)}{45^o} - 1 \leq 0 \qquad g_E(\mathbf{X},t) = \frac{\psi(t)}{45^o} - 1 \leq 0 \tag{11}$$

which are collapsed into the point constraints

$$\begin{aligned} g_8(\mathbf{X}) &= \int_0^T < g_D(\mathbf{X};t) >^2 \, dt \leq 0 \\ g_9(\mathbf{X}) &= \int_0^T < g_E(\mathbf{X};t) >^2 \, dt \leq 0 \end{aligned} \tag{12}$$

6. ADS-33 requires that the maneuver be completed on the centerline. To satisfy this requirement, first the following quantity is defined:

$$y_{ave}^2 = \frac{1}{x_{max} - 1500} \int_{1500}^{x_{max}} y^2 \, dx \tag{13}$$

which is the average value of the square of the lateral displacement from the centerline after the completion of the maneuver. The quantity x_{max} is the

distance at the end of the maneuver. The simulation is carried out for a prescribed time, but the speed of the helicopter is not necessarily constant, and therefore the actual value of x_{max} is not fixed and depends on the particular maneuver. The constraint then becomes

$$g_{10}(\mathbf{X}) = \frac{y_{ave}}{2} - 1 \leq 0 \qquad (14)$$

which requires that the average lateral displacement be less than 2 feet.

4. Preliminary step — Trajectory matching

Some optimization algorithms require that the initial solution be feasible (i.e., such that all the constraints are satisfied); others can start from an infeasible solution (i.e., one that violates one or more constraints) and seek a feasible one. In general, however, it is advisable to start from a feasible solution. Therefore, the objective of this preliminary step is to generate such a feasible solution by matching a preassigned trajectory that satisfies all the constraints. This trajectory is defined as follows:

$$y_D(x) = \begin{cases} 75\left[2\left(\frac{x}{500}\right)^3 - 3\left(\frac{x}{500}\right)^2\right] & x \leq 500 \\ 75\left[1 - 6\left(\frac{x-500}{500}\right)^2 + 4\left(\frac{x-500}{500}\right)^3\right] & 500 \leq x \leq 1000 \\ 75\left[1 - 3\left(\frac{x-1000}{500}\right)^2 + 2\left(\frac{x-1000}{500}\right)^3\right] & 1000 \leq x \leq 1500 \\ 0 & x \geq 1500 \end{cases} \qquad (15)$$

plus $z_D(x) = 0$. This trajectory satisfies all the constraints except for those that enforce a minimum airspeed, Eq. (7), and bounds on the heading, Eq. (12). The objective function for this step minimizes the deviation of the actual trajectory from the required one, and includes the constraints $g_5(\mathbf{X}), g_8(\mathbf{X})$ and $g_9(\mathbf{X})$ in the form of penalty functions. The formulation for this step can be obtained from the general formulation described in the previous section by removing all the constraints, and defining the objective function as:

$$F(\mathbf{X}) = \int_0^T \left[(y - y_D)^2 + z^2\right]^{1/2} dt + r_5 g_5(\mathbf{X}) + r_8 g_8(\mathbf{X}) + r_9 g_9(\mathbf{X}) \rightarrow \min \qquad (16)$$

The penalty parameters r_5, r_8, and r_9 are all set equal to one. Therefore, the solution of this step requires the *unconstrained* minimization of the augmented objective function $F(\mathbf{X})$.

In principle, the optimization could be carried out only until the solution satisfies all the constraints of the general formulation, and then switch to the desired constrained optimization. However, in this section the optimization will be performed until convergence, both to explore some important general features of the optimization process, and also because this step provides a different approach to the inverse simulation problem with fixed trajectory. The unconstrained optimization problem is solved using a BFGS [17] algorithm, as implemented in the optimization code DOT [18].

Practical implementation issues

Problems due to aircraft instabilities

Without automatic stabilization all helicopters are unstable in hover. Some configurations, like that of the present study, remain unstable in forward flight. This can affect the trajectory optimization, as evidenced by Figure 2 which shows an inverse simulation carried out for 14 seconds of simulated time. The vector $\mathbf{X}$ contains the four control inputs at one second intervals, for a total of 56 elements. The figure shows the converged solution, which clearly does not match the required trajectory very well.

Figure 3 helps explain the problem. The top plot shows the portion of the search direction $\mathbf{S}$ corresponding to the lateral cyclic pitch θ_{1c} at the last iteration of optimization. Recall [17] that the optimization is composed of two basic steps, that is, the determination of a search direction $\mathbf{S}$, and a one-dimensional minimization of the objective $F(\mathbf{X})$ along $\mathbf{S}$ that updates the design $\mathbf{X}$ according to $\mathbf{X} = \mathbf{X}_0 + \alpha\mathbf{S}$, where α is the independent variable of the 1-D minimization. Therefore, the figure shows that the optimizer would like to decrease θ_{1c} for the first 4 seconds, i.e., move the stick further to the right. Figure 2 shows that instead the stick should be moved further *to the left* to match the desired trajectory. Therefore, the optimizer generates the wrong maneuver. The gradient of $F(\mathbf{X})$ with respect to the θ_{1c} inputs is shown at the bottom of Figure 3. To obtain the gradients using finite difference approximations each control is slightly increased, and therefore the figure shows the changes in the objective function caused by a small perturbation of lateral stick to the left. (Note that the search direction is close to a scaled version of the negative of the gradient.)

The objective function, i.e., the discrepancy from the required trajectory, increases with larger left stick inputs at the beginning of the maneuver. This apparent inconsistency can be explained by considering Figure 4. The figure shows one of the perturbations of lateral cyclic used to calculate the gradient of $F(\mathbf{X})$, namely that at time $t = 3$ sec, and the corresponding perturbation of the trajectory y. Because the helicopter is unstable, the triangular impulse produces relatively large perturbations toward the end of the maneuver, and much smaller ones in the first few seconds. Therefore, the component of the

gradient reflects overwhelmingly the end of the maneuver and produces the unrealistic results mentioned before. If the helicopter dynamics had been well damped, the effect of the perturbation of lateral cyclic would have been confined to the instants immediately following the input.

The problem can be eliminated by performing the optimization over overlapping segments of the trajectory rather than over the entire trajectory. In Figure 5 each segment lasts 3 seconds, and the last two seconds of a given segment overlap with the first two of the next. The trajectories of the first second of each segment are then joined together and provide the required complete trajectory. The design vector $\mathbf{X}$ contains only the controls corresponding to the 3 seconds of the segment. Because the controls are updated every 0.5 seconds the total number of design variables is 24. Therefore, the original optimization problem has been replaced by a sequence of smaller problems that, as a group, provide the complete solution. Figure 5 shows that the agreement between actual and required trajectories is excellent, except for the first 2-3 seconds in which the required trajectory perhaps requires too high a lateral load factor. The figure also shows the trajectories calculated over each segment. One of them is marked with a thicker line for illustration. The trajectory of Figure 5 satisfies the criteria of ADS-33D (except obviously for the reduction to two turns rather than four).

The length of each segment and the extent of the overlap of consecutive segments are likely to depend on the dynamics of each aircraft configuration, especially if there are unstable modes. The values used in this study were the longest length and the shortest overlap that would reliably work in all cases, but a study of different aircraft configurations was not performed. The configuration used in this study (small size aircraft, hingeless rotor, unstable) is probably a "worst case scenario", and therefore the 3-second length and 2-second overlap are likely to be a safe choice in most cases.

Effect of numerical tolerances

An important practical issue is the accuracy of the gradients, which depends on the finite difference step size. In this study, the integration of the equations of motion of the helicopter is carried out using the variable-step, variable-order solver DASSL [15], which attempts to satisfy user-defined local error tolerances. Therefore, the finite difference step size must be selected consistently with these error tolerances. The interaction between gradient calculation and the integration of the equations of motion is an important issue in trajectory optimization: Ref. [19] points out that less sophisticated fixed-step/fixed-order ODE solvers can often be more efficient overall because they don't introduce numerical noise in the gradients.

However, this problem cannot be avoided in helicopter applications, if one wants to devise inverse simulation algorithms that can be used with the most sophisticated helicopter simulation models. In these models, the mathematical expressions can be so lengthy that it may not be convenient to include all the terms in traditional mass, damping, and stiffness matrices, but it is necessary to leave many of them in a generic form as an external nonlinear forcing function (see for example Ref. [20]) on the right-hand-side of the governing equations. Therefore, the ODE solver needs to perform Newton-Raphson type iterations at each integration step, whether the step size is fixed [21] or variable [15, 16], and this brings back the need to define a convergence criterion through an error tolerance.

In the present study, the relative and absolute local errors used for the ODE solution are both equal to 10^{-5}. This value offers a good compromise between accuracy and computational effort [16]. To explore the effect of numerical tolerances, the optimization was performed with several values of the step size used in the finite difference calculation of the gradients. Each design variable was increased by a given relative amount e_R. If the absolute value of the perturbation was smaller than a given value e_A, the value e_A was used instead. Figure 6 shows the results of the optimization for $e_R = 10^{-1}, 10^{-2}, 10^{-3}$, and 10^{-4}, and $e_A = 0.1 e_R$ in all cases. Both the lateral displacement $y(x)$ and the vertical displacement $z(x)$ are shown. The curves for the first three values of e_R are essentially superimposed in the scale of the figure. The corresponding values of the objective function $F(\mathbf{X})$ are 44.9, 12.8, and 40.6 respectively, and therefore $e_R = 10^{-2}$ gives the best accuracy in this case. When $e_R = 10^{-4}$ the match between actual and required trajectory is poor, the value of the objective is 959.8, and the 18 seconds are not sufficient to complete the maneuver. The ADS-33D criteria would not be satisfied. It is clear that calculating the gradients with a finite difference step comparable to the local error tolerance for the ODE solver leads to poor results. On the other hand, relatively large step sizes do not degrade seriously the accuracy of the solution, and even a size of 10% of the independent variables (with an absolute lower bound of 0.01) gives good results. All the trajectories presented in the rest of the paper have been obtained with $e_R = 10^{-2}$ and $e_A = 10^{-3}$. These values are also likely to be adequate for more general cases (i.e., different maneuvers or aircraft configurations), if the solution of the governing equations is obtained with local error tolerances of 10^{-5} or tighter.

Multiple acceptable trajectories

When acceptable trajectories are defined indirectly, through a set of criteria, multiple solutions can exist. Figure 7 shows three acceptable solutions for the simplified slalom maneuver, obtained by matching three different trajectories. The "baseline" trajectory is that of Eq. (15). For the other two, the constant 75 in Eq. (15) is replaced by 55 and 95. This corresponds to lateral excursions from the centerline of 55 and 95 ft respectively, and therefore almost to the limits prescribed by ADS-33.

For each curve in the figure, the dashed line indicates the required trajectory, the solid line the actual trajectory. In all cases the match is very good, especially after the first 2-3 seconds. The altitude changes are very small in all cases. The lower plot in Figure 7 shows the time histories of the roll angle ϕ. These values are taken with respect to the trim state. Differences of 20^o or more of roll angle among the trajectories can be easily seen. The time histories of lateral and longitudinal cyclic are presented in Figure 8. It should be noted that all the pitch values presented in this paper are perturbations from their trim values. Differences in magnitude, phase, and frequency of the inputs are evident, especially in the first half of the maneuver. Overall, these results show that the slalom requirements of ADS-33D can be satisfied by quite different maneuvers.

Multiple acceptable trajectories can also be due to the presence of local minima in the trajectory optimization problem. To study this issue, the trajectory matching problem was repeated three times for the trajectory of Eq. (15), with different initial guesses for the control time histories. The differences among the trajectories are minimal (the curves would be superimposed in the scale of Figure 5), and the three altitude profiles do not differ by more than 2 ft throughout the maneuver. However, some difference can be seen in the time histories of the roll angle ϕ, shown in Figure 9. For example, the roll reversal to clear the first marker at 500 ft, from about -50 to about 50 degrees, occurs smoothly in trajectory 3. Instead, in trajectory 1 the roll to the right is too fast, and there is a short left roll maneuver that reduces ϕ by about 20 degrees before the roll to the right resumes. A similar maneuver can be seen in trajectory 2. The same qualitative differences among trajectories can be seen later, when the helicopter starts rolling to the left before clearing the marker at 1000 ft. Here, both trajectory 1 and 2 are smooth, whereas a brief reversal is visible in trajectory 3.

The corresponding inputs of lateral cyclic are shown in Figure 10. The inputs for trajectory 1 have the largest excursions of the three in the initial seconds of the slalom, whereas those for trajectory 3 are the largest before the second marker. In the present study no upper bounds were placed on magnitude and rate of the pitch inputs, and therefore the solution does not take control saturation into account. Because each design variable is the value of one control at a given time, this could be easily done by placing bounds on the magnitude of the design variables, alone or in combination. Magnitude and rates in Figure 10 do not appear unrealistically high, but in general it will be prudent to include saturation constraints.

The harmonics of the lateral cyclic input are shown in Figure 11. The slalom is completed in about 14 seconds. If this is taken as the period of the maneuver, then the corresponding frequency is about 0.4 rad/sec. The largest contribution is at twice this frequency because of the inputs required to clear the two markers. A second peak is visible at a frequency of about 2 rad/sec, which is near the frequency of the Dutch roll mode in steady straight flight. The analysis of the pilot input spectrum can provide important information on the handling qualities characteristics of the aircraft in the maneuver. In general, a higher frequency content is associated with increased pilot workload and degraded handling qualities (very interesting discussions of this issue can be found in Padfield *et al.* [22] and Blanken *et al.* [23]).

5. Trajectory determination through constrained optimization

The slalom demonstration maneuver in ADS-33D does not require that a specific trajectory be matched, as long as the constraints described in Section 3 are satisfied. As a consequence, an entire *family* of trajectories will generally exist, and it will be possible to single out specific ones to address a variety of different objectives. In this section, for example, the goal is to study ADS-33D compliant slalom maneuvers that maximize flight speed, with the idea that these are going to be the most aggressive maneuvers. Mathematically, the objective function will then be the average speed over each 3-second segment, that is:

$$F(\mathbf{X}) = -k \int V \, dt \rightarrow \min \tag{17}$$

where k is simply a constant scale factor to keep the size of $F(\mathbf{X})$ reasonably small. The constraints are those described in Section 3.

Two additional constraints keep the trajectory $y(x)$ within the corridor shown in Figure 12. The curve marked y_{75} is that defined by Eq. (15), those marked with y_{50} and y_{100} are obtained from Eq. (15) by replacing the constant 75 with 50 and 100 respectively. The left limit of the trajectory is the upper curve in Fig. 12, defined for every x as the smallest among y_{50}, y_{100}, $y_{75} \pm 10$ ft for $x < 1000$ ft, and $y_{75} \pm 5$ ft for $x \geq 1000$ ft. The largest of those values defines the right limit of the trajectory. These trajectory constraints are implemented using the bracket functions, and have a form similar to that of Eq. (7). The corridor is necessary because otherwise the optimization in the first 3-second segment might not be aware of the presence of the marker at 500 ft, and would not begin the first turn to the left. Similarly, the 1000 ft marker may not be reached within 3 seconds of clearing the 500 ft marker, and therefore the optimizer would delay the preparation for its clearing. With those that define the required corridor, the total number of constraints of the optimization problem is 12.

The constrained optimization problem is solved using a modified method of feasible directions (MMFD), as implemented in the optimization code DOT [18]. DOT can also solve constrained optimization problems using sequential linear programming (SLP) or sequential quadratic programming (SQP) algorithms. Limited numerical experimentation showed that SLP requires a

very careful management of move limits on the design variables, and sometimes fails. SQP proved slightly more robust, but required about 3 times the computational effort of MMFD. The MMFD algorithm proved very reliable and reasonably efficient.

The results of the optimization are presented in Figures 13 through 15. Each contains several curves, corresponding to different initial velocities for the maneuver. In fact, the first optimization, carried out for an entry speed of 60 kts, revealed that this initial speed could not be increased by more than 1-2 knots in each segment. The optimization was repeated for an entry speed of 65 kts, and then for speeds raised in 2 knot increments until, at 71 knots, it was no longer possible to find a feasible solution. Although the slalom entry speed could itself be a design variable in the optimization, this was not done in the present study.

The various trajectories are shown in Figure 13. As the speed increases, the turns become wider until, at 71 knots, it is not possible to remain within 100 feet from the centerline at $x = 500$ ft. The time required to complete the maneuver, i.e., to cross the $x = 1500$ ft line, is also indicated in the figure, and ranges from 14.9 sec to 13.4 sec as the entry speed increases from 60 to 69 knots. In all cases the optimization increases speed by about 1-2 knots over the entry speed. Not surprisingly, the plots of $z(x)$ indicate that the optimum maneuvers make the helicopter lose altitude, to trade potential for kinetic energy and increase speed. Figure 14 shows the time histories of the roll angle ϕ. Clearly, as the maneuver becomes more aggressive, the peak values of the roll angle increase; the increment in the initial turn is of almost 20 degrees. In the final seconds of the maneuver the changes in ϕ become much more pronounced as the speed increases.

Information on constraint activity is presented in Table 1. Each column refers to an entry speed, each row to a 3-second optimization segment. Only four constraints ever become active or violated, namely the lower bound V_{min} on flight speed, Eq. (6), the upper bound on altitude loss z_{max}, Eq. (9), and those that define the corridor of Figure 12. The z_{max} constraint is active for several segments at all entry speeds, confirming that the optimizer tries to make the helicopter lose altitude to gain energy. The V_{min} constraint becomes active only for an entry speed of 60 kts. It does so at the beginning of the maneuver (it is actually violated slightly in the first segment), when the helicopter has not yet been able to accelerate, and after the 1000 ft marker has been cleared. At higher speeds, the helicopter stays in the corridor with greater difficulty, especially around and between the markers, as clearly shown by the constraint activity. Finally, for an entry speed of 71 knots it becomes impossible for the helicopter to stay in the corridor and to clear the 500 ft marker with a lateral displacement of less than 100 ft; after two consecutive infeasible segments the optimization is terminated.

The harmonic content of the lateral cyclic inputs is shown in Figure 15, which includes the values of the fundamental frequency, defined as the inverse of the time required to complete the maneuver. As in the trajectory matching solutions, the largest contributions are at twice the fundamental frequency because of the inputs required to clear the two markers. As the maneuver becomes more aggressive, higher frequency contributions develop. A peak appears at about 2 rad/sec, corresponding to the Dutch roll mode in steady straight flight.

Multiple solutions

If the design space is not convex, optimization problems may have multiple solutions corresponding to local minima. To determine whether this is the case in the present study, the maximum speed problem with an entry speed of 69 knots was solved three times, each with a different initial guess for the pilot inputs. The resulting trajectories are shown in Figure 16. Clearly, the optimum trajectory depends on the initial guess, indicating the existence of local minima. The corresponding times required to fly the slalom differ by almost a second, or slightly less than 10% of the total time. The lateral cyclic inputs for each solution are shown in Figure 17. The general trend is the same for the three solutions, but there is little overlap, and there are occasional differences of 4 degrees or more. Whether the nonuniqueness of the optimal solution is a practical problem will depend on the reasons for performing the inverse simulation. For handling qualities studies, the scatter in the solutions may help predict the amount of scatter in pilot ratings to be expected for a given maneuver. On the other hand, if the inverse simulation is used for simulation validation, then additional constraints may have to be placed on the solution to make it unique.

6. Summary and Conclusions

This paper presented an inverse simulation methodology based on numerical optimization. The methodology was applied to a slalom maneuver defined through a set of criteria, rather than a prescribed path, as is the case in the ADS-33D handling qualities specification. The inverse simulation was formulated as an optimization problem with trajectory and dynamic constraints, pilot inputs as design variables, and an objective function that depends on the problem being solved. A maximum speed solution was considered in the paper. A feasible initial solution can be obtained by matching a prescribed trajectory designed to satisfy all the constraints of the original problem. This trajectory matching problem was formulated as an unconstrained optimization, which can be independently used as a new technique for the traditional problem of inverse simulation with preassigned trajectory.

The main conclusions of the present study are:

1. Numerical optimization is a reliable and flexible tool for inverse simulation, both when the required tra-

jectory is prescribed explicitly and when it is defined indirectly through geometric and dynamic constraints. For unstable or lowly damped configurations the optimization is best performed on overlapping segments, rather than in a single pass covering the entire maneuver.

2. The inverse simulation problem with preassigned trajectory can have multiple solutions. The multiple solutions of the slalom maneuver identified in this study all matched very well the preassigned trajectory of the aircraft center of gravity, but showed noticeable differences in the helicopter dynamics and in the required pilot inputs.

3. When the trajectory is defined indirectly, as is the case in the ADS-33D specification, there is not a single acceptable trajectory, but rather an entire family. Selecting specific members of this family, by specifying an objective function to be minimized, results in a constrained optimization problem that can itself have multiple solutions, corresponding to local minima in the design space. These solutions satisfy all the constraints, but differ in the time histories of the aircraft dynamics and of the pilot inputs.

4. Whether or not the nonuniqueness of the optimal solutions is practically significant will depend on the reasons for performing the inverse simulation. For handling qualities studies, it may provide an indication of the amount of scatter in the pilot ratings to be expected for a given aircraft and a given maneuver. If the inverse simulation is used as part of a simulation validation, then additional constraints may have to be placed on the solution to make it unique.

Acknowledgments

This research was supported by the National Rotorcraft Technology Center, under the Rotorcraft Center of Excellence Program, Technical Monitor Dr. Yung Yu.

References

[1] Anonymous, "Aeronautical Design Standard ADS-33D, Handling Qualities Requirements for Military Rotorcraft," U. S. Army Aviation and Troop Command, St. Louis, MO, July 1994.

[2] McKillip, R. M., Jr., and Perry, T. A., "Helicopter Flight Control System Design and Evaluation Using Controller Inversion Techniques," *Journal of the American Helicopter Society*, Vol. 37, No. 1, January 1992, pp. 66-74.

[3] Thomson, D. G., and Bradley, R., "Development and Verification of an Algorithm for Helicopter Inverse Simulation," *Vertica*, Vol. 14, No. 2, 1990, pp. 185-200.

[4] Bradley, R., and Thomson, D. G., "Handling Qualities and Performance Aspects of the Simulation of Helicopters Flying Mission Task Elements," *Proceedings of the Eighteenth European Rotorcraft Forum*, Avignon, France, Sept. 1992, pp. 139.1-139.15.

[5] Whalley, M. S., "Development and Evaluation of an Inverse Solution Technique for Studying Helicopter Maneuverability and Agility," NASA TM 102889 and USAAVSCOM TR 90-A-008, July 1991.

[6] Hess, R. A., Gao, C., and Wang, S. H., "Generalized Technique for Inverse Simulation Applied to Aircraft Maneuvers," *Journal of Guidance, Control, and Dynamics*, Vol. 14, No. 5, Sept.-Oct. 1991, pp. 920-926.

[7] Hess, R. A., Gao, C., "A Generalized Algorithm for Inverse Simulation Applied to Helicopter Maneuvering Flight," *Journal of the American Helicopter Society*, Vol. 38, No. 3, Oct. 1993, pp. 3-15.

[8] Rutherford, S., and Thomson, D. G., "Improved Methodology for Inverse Simulation", *The Aeronautical Journal*, Vol. 100, No. 993, Mar. 1996, pp. 79-86.

[9] de Matteis, G., de Socio, L. M., and Leonessa, A., "Solution of Aircraft Inverse Problems by Local Optimization," *Journal of Guidance, Control, and Dynamics*, Vol. 18, No. 3, May-June 1995, pp. 567-571.

[10] Lee, S., and Kim, Y., "Time-Domain Finite Element Method for Inverse Problem of Aircraft Maneuvers," *Journal of Guidance, Control, and Dynamics*, Vol. 20, No. 1, Jan.-Feb. 1997, pp. 97-103.

[11] Borri, M., Bottasso, C. L., and Montelaghi, F., "Numerical Approach to Inverse Flight Dynamics," *Journal of Guidance, Control, and Dynamics*, Vol. 20, No. 4, July-Aug. 1997, pp. 742-747.

[12] Yip, K. M., and Leng, G., "Stability Analysis for Inverse Simulation of Aircraft," *The Aeronautical Journal*, Vol. 100, No. 1007, June-July 1998, pp. 345-351.

[13] Chen, R.T.N., and Jeske, J.A., "Kinematic Properties of the Helicopter in Coordinated Turns," NASA Technical Paper 1773, Apr. 1981.

[14] Celi, R., "Hingeless Rotor Dynamics in Coordinated Turns", *Journal of the American Helicopter Society*, Vol. 36, No. 4, Oct. 1991, pp. 39-47.

[15] Brenan, K. E., Campbell, S. L., and Petzold, L. R., *The Numerical Solution of Initial Value Problems in Differential-Algebraic Equations*, Elsevier Science Publishing Co., New York, 1989.

[16] Celi, R., "Implementation of Rotary-Wing Aeromechanical Problems Using Differential-Algebraic Equation Solvers," submitted for publication in the *Journal of the American Helicopter Society.*

[17] Vanderplaats, G. N., *Numerical Optimization Techniques for Engineering Design: With Applications*, McGraw-Hill, New York, 1984.

[18] Vanderplaats, G. N., *DOT–Design Optimization Tools, User's Manual*, VMA Engineering, Inc., Goleta, CA, May 1995.

[19] Betts, J. T., "Survey of Numerical Methods for Trajectory Optimization," *Journal of Guidance, Control, and Dynamics*, Vol. 21, No. 2, Mar.-Apr. 1998, pp. 193-207.

[20] Rutkowski, M., Ruzicka, G. C., Ormiston, R. A., Saberi, H., and Jung, Y., "Comprehensive Aeromechanics Analysis of Complex Rotorcraft Using 2GCHAS," *Journal of the American Helicopter Society*, Vol. 40, No. 4, Oct 1995, pp. 3-17.

[21] Panda, B., "A Robust Direct-Integration Method for Rotorcraft Maneuver and Periodic Response," *Journal of the American Helicopter Society*, Vol. 37, (3), July 1992, pp. 83-85.

[22] Padfield, G. D., Jones, J. P., Charlton, M. T., Howell, S. E., and Bradley, R., "Where Does the Workload Go When Pilots Attack Manoeuvres?, An Analysis of Results from Flying Qualities Theory and Experiment," *Proceedings of the 20th European Rotorcraft Forum*, Amsterdam, Holland, October 1994.

[23] Blanken, C. L., Pausder, H.-J., and Ockier, C. J., "An Investigation of the Effects of Pitch-Roll (De)Coupling on Helicopter Handling Qualities," NASA TM 110349 and USAATCOM TR 95-A-003, May 1995.

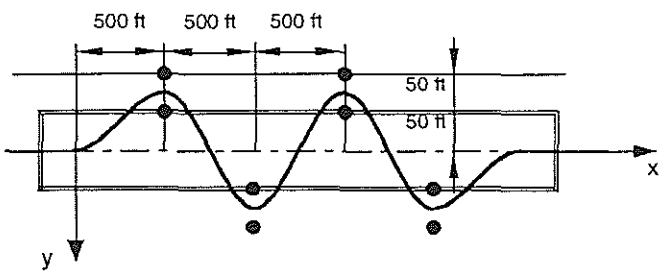

Figure 1: Slalom maneuver, from Paragraph 4.2.6 of ADS-33D [1].

Time (sec)	Entry velocity (kts) 60	65	67	69	71
0-3	$\underline{V_{min}}$ $\underline{z_{max}}$ $\underline{y_U}$	y_U	z_{max}	none	y_U
1-4	V_{min} z_{max}	z_{max} y_U	z_{max}	none	y_U
	y_U	y_L	z_{max}	none	y_U
2-5	z_{max}	none	none	z_{max}	z_{max}
3-6	none	none	y_L	y_L	V_{min}, z_{max} $\underline{y_U}$, $\underline{y_L}$
4-7	none	y_L	z_{max}	z_{max} y_L	V_{min}, z_{max} $\underline{y_U}$, $\underline{y_L}$
5-8	z_{max}	z_{max} y_L	y_U y_L	z_{max} y_L	infeasible
6-9	none	z_{max} y_L	y_U y_L	z_{max} y_U y_L	↓
7-10	z_{max} y_U	none	y_U	y_U	
8-11	z_{max}	z_{max}	y_U	y_U	
9-12	V_{min} z_{max}	z_{max}	z_{max} y_U	y_U	
10-13	V_{min} z_{max}	z_{max} y_L	y_U	none	
11-14	V_{min} z_{max}	none	z_{max}	z_{max}	
12-15	z_{max}	z_{max}	z_{max} y_L	y_U	
13-16	z_{max}	none	z_{max} y_L	z_{max}	
14-17	none	z_{max} y_U	z_{max} y_L	y_U	
15-18	z_{max} y_U y_L	z_{max}	z_{max}	z_{max} y_U	

Key:
V_{min} → lower bound on speed, Eq. (6)
z_{max} → upper bound on altitude loss, Eq. (9)
y_U → upper bound on lateral displacement
y_L → lower bound on lateral displacement

Table 1: Active constraints for the maximum speed slaloms; underlined constraints are violated.

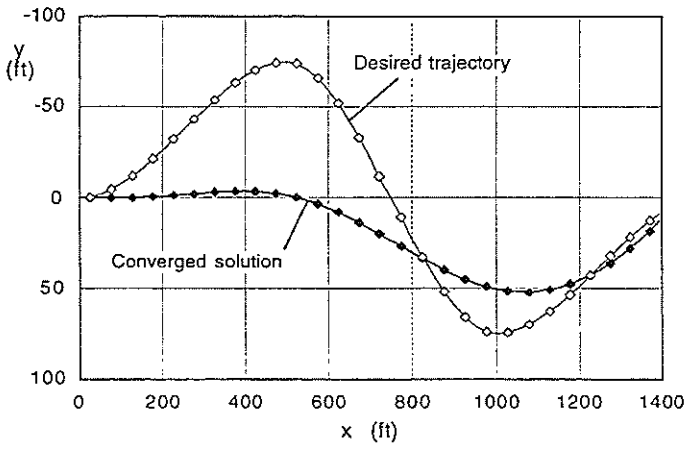

Figure 2: Solution when the complete pilot input time history is included in the optimization; the markings on the curves are at 0.5 second intervals.

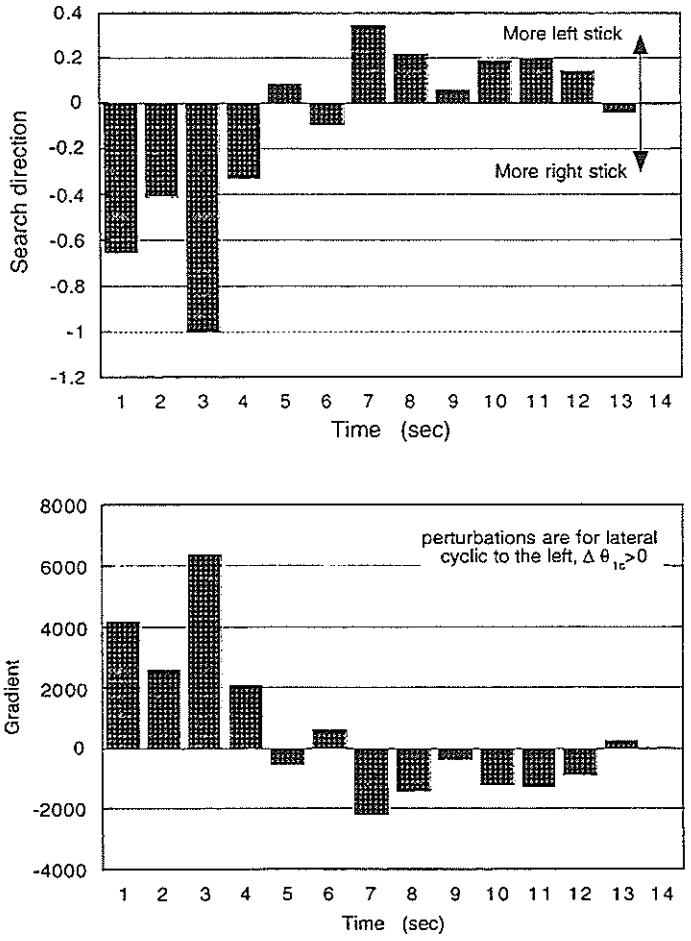

Figure 3: Search direction (top) and gradient of the objective function (bottom) for lateral cyclic pitch.

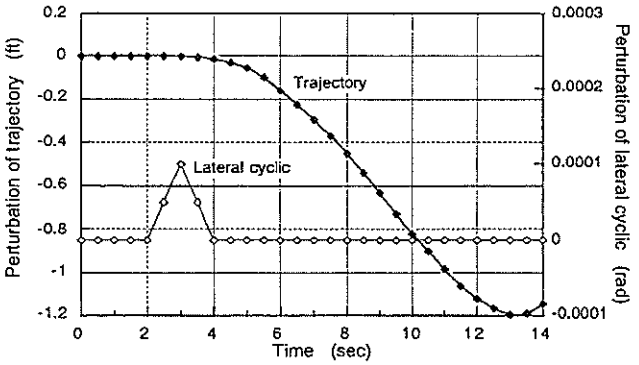

Figure 4: Solution when the complete pilot input time history is included in the optimization; the markings on the curves are at 0.5 second intervals.

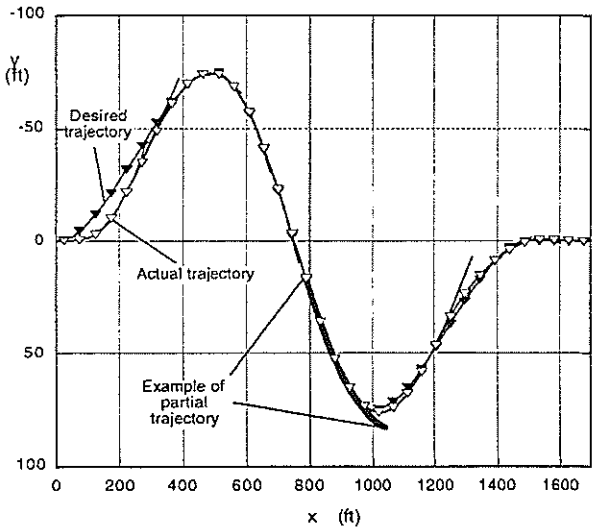

Figure 5: Optimization with overlapping segments; open symbols: actual trajectory, closed symbols: desired trajectory.

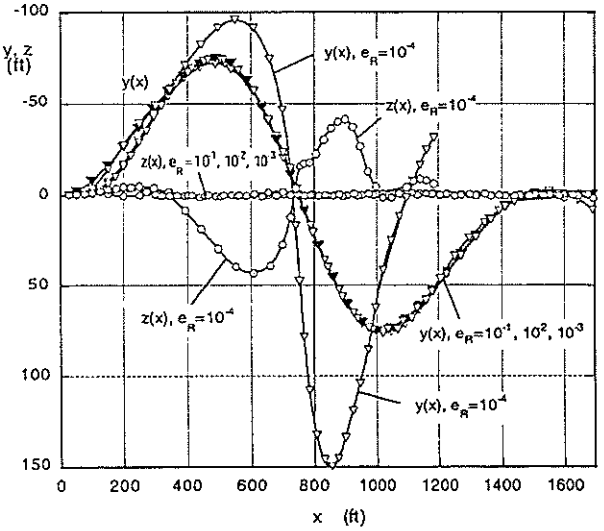

Figure 6: Effect on the final trajectory of the finite difference step in gradient calculations.

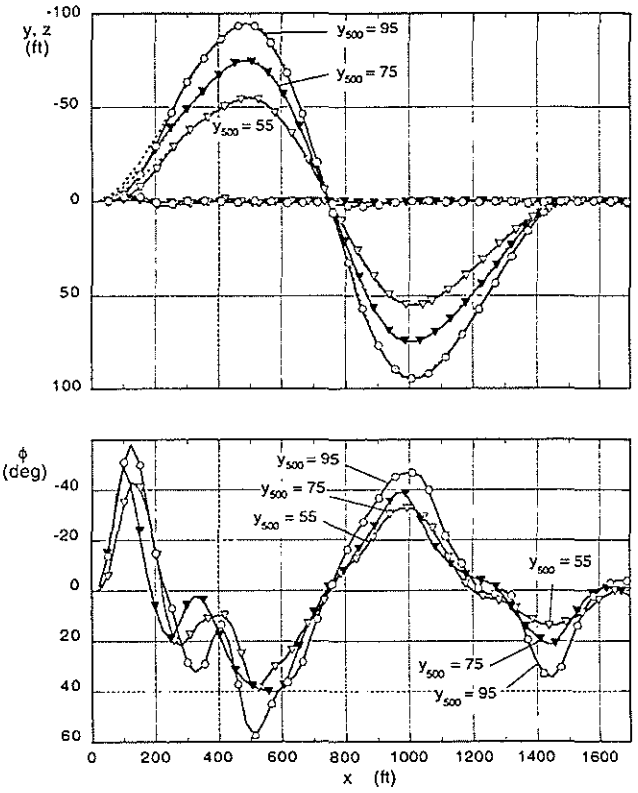

Figure 7: Three acceptable trajectories for the slalom maneuver.

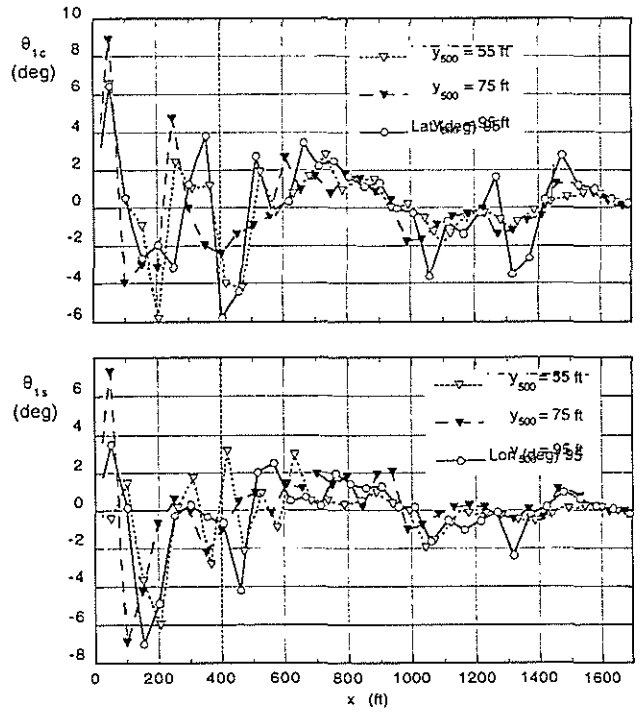

Figure 8: Cyclic pitch inputs for three acceptable trajectories for the slalom maneuver.

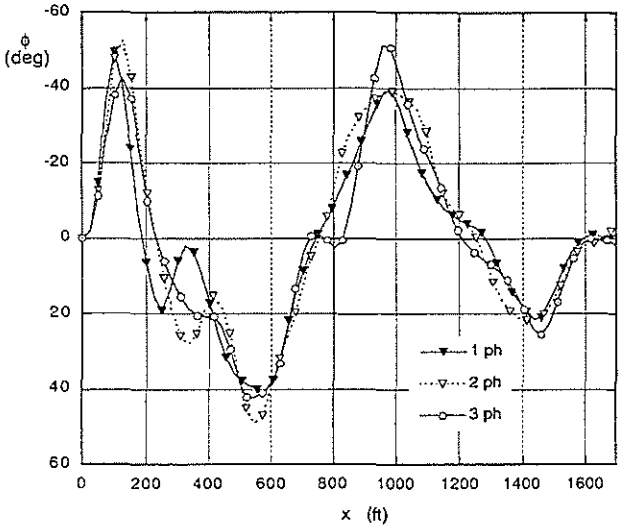

Figure 9: Time histories of roll angle ϕ for three solutions of the trajectory matching problem; lateral displacement ± 75 ft from centerline.

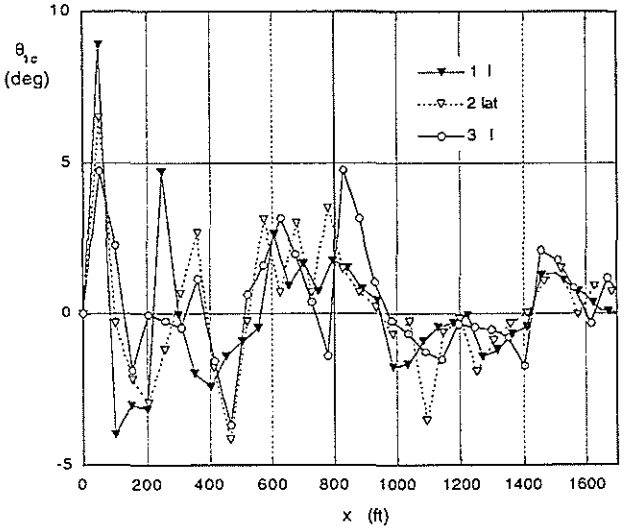

Figure 10: Time histories of lateral cyclic pitch θ_{1c} for three solutions of the trajectory matching problem; lateral displacement ± 75 ft from centerline.

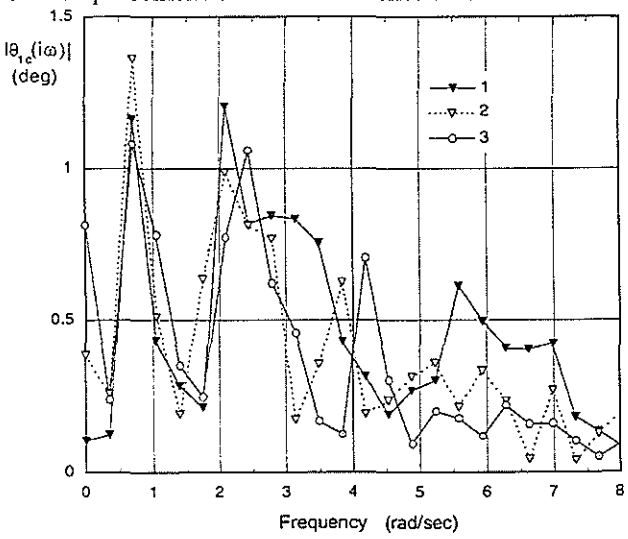

Figure 11: Harmonics of lateral cyclic pitch θ_{1c} for three solutions of the trajectory matching problem; lateral displacement ± 75 ft from centerline.

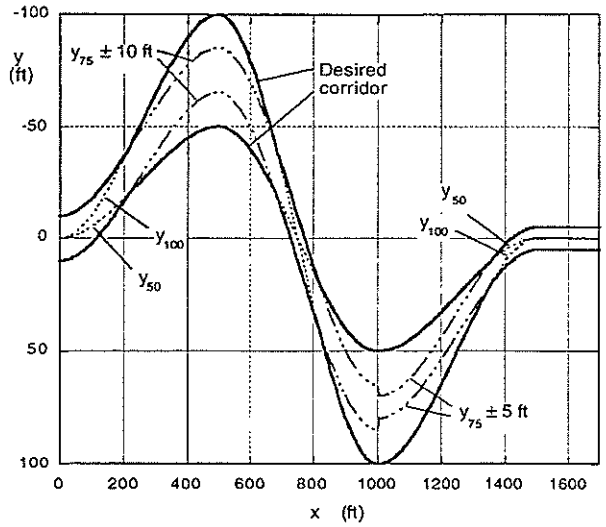

Figure 12: Desired trajectory bounds for constrained trajectory optimization, top view.

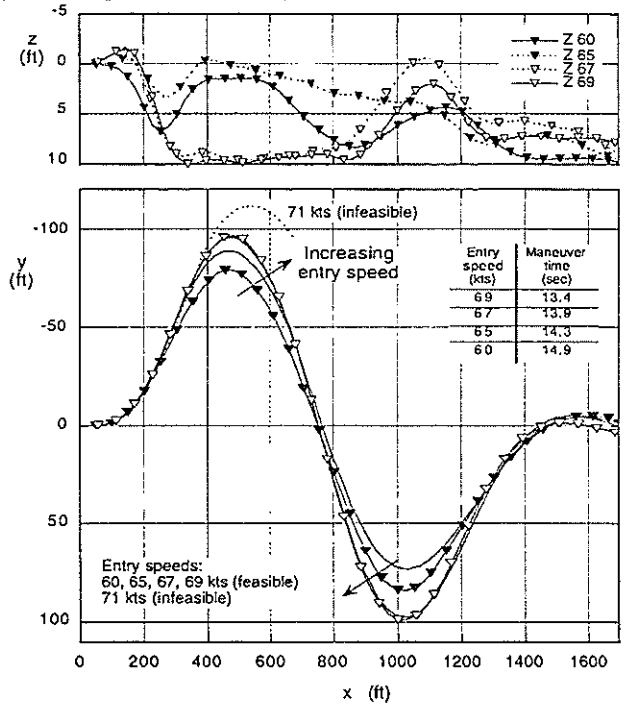

Figure 13: Maximum speed trajectories for various slalom entry speeds.

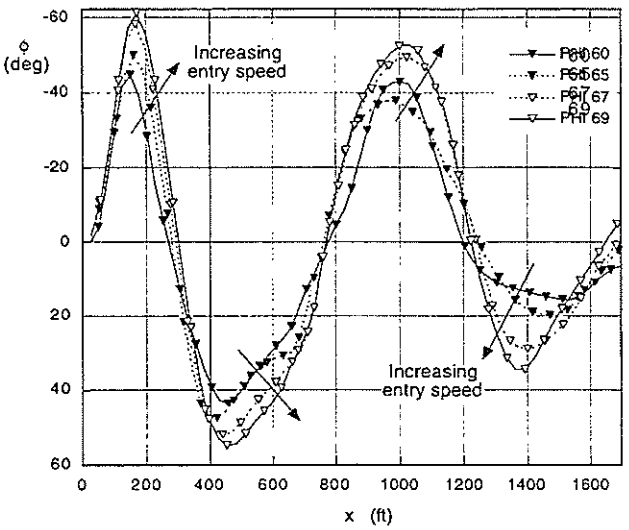

Figure 14: Time histories of roll angle ϕ for various slalom entry speeds.

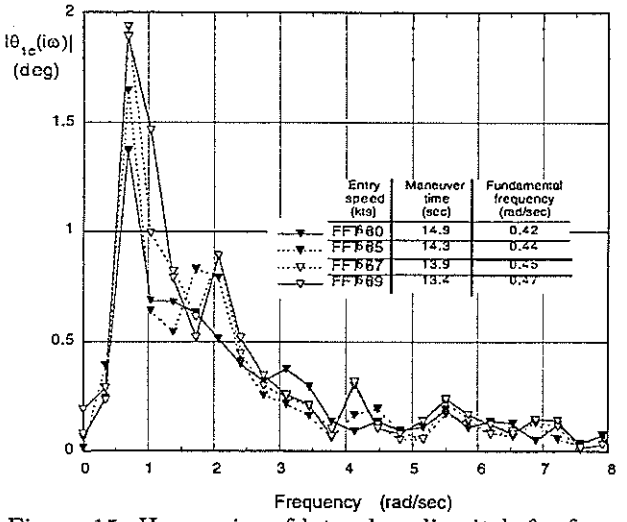

Figure 15: Harmonics of lateral cyclic pitch θ_{1c} for various slalom entry speeds.

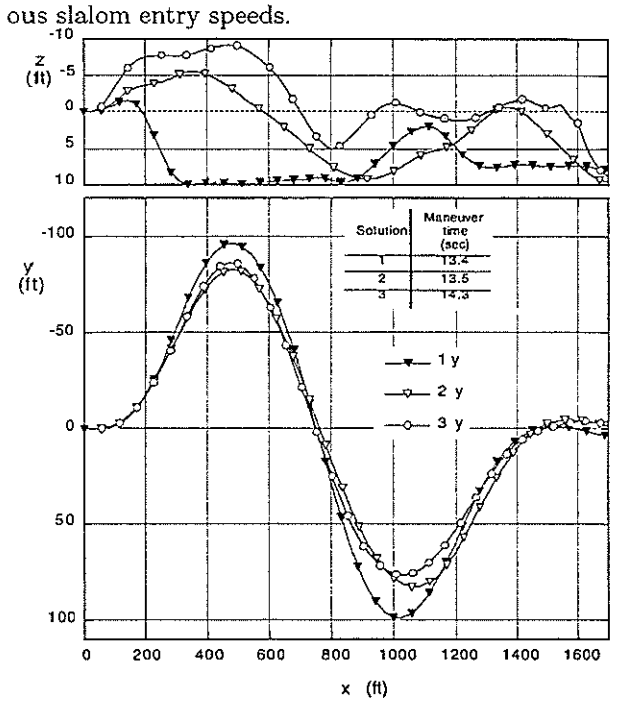

Figure 16: Solutions of the maximum speed optimization for three different initial guesses; slalom entry speed $V = 69$ kts.

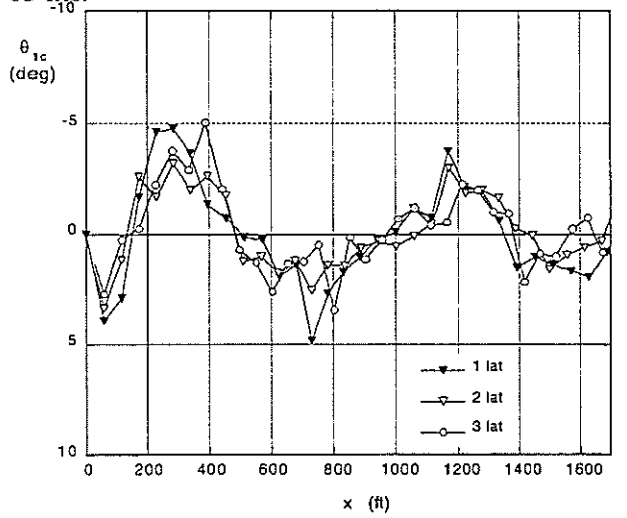

Figure 17: Time histories of lateral cyclic pitch θ_{1c} for three solutions of the maximum speed slalom; slalom entry speed $V = 69$ kts.